Numerical Study on W-type Collecting Plates with Multiple Corona Electrodes of Electrostatic Precipitators*

Mo'ath Bani Fayyad[1 [0000−0001−8105−725X]], Angel Asipuela González[1,2 [0000−0001−8098−8714]], and Iváncsy Tamás[1,3 [0000−0003−3367−2869]]

[1] Department of Electric Power Engineering, Faculty of Electrical Engineering and Informatics, Budapest University of Technology and Economics
mbanifayyad@edu.bme.hu
[2] gabriel.bme_2020@edu.bme.hu
[3] ivancsy.tamas@vet.bme.hu

Abstract. The optimal arrangement of collecting plates and corona wires considerably impacts the collection efficiency of Electrostatic Precipitators (ESPs). Many experts are striving to improve existing models in a variety of methods. This research aims to examine the effects of using multiple corona wires with W-type collecting plates on the properties of electrostatic precipitators. Three different types of corona wire arrangements with W-type collecting plates were modeled and compared with Flat Plates (FPs) to evaluate the effect of using multiple corona electrodes on the electrical field distribution, space charge density distribution, current density distribution, and particle collection efficiency.

Keywords: Electrostatic precipitator · Corona discharge · Corona wire arrangement · Numerical simulation · Particle collection efficiency.

1 Introduction

In recent years, particulate emissions have advanced to the top of the global priority list [1]. A wide range of industrial applications relied on electrostatic precipitators (ESPs) to remove particles, such as power plants, metallurgical industries for copper, lead, and zinc production, the steel industry, aluminum production smelters (including cement production), pulp and paper mills, chemical manufacturing, the processing of fuel gases, and the production of glass, to name a few examples [2–5]. ESPs are distinguished by their high collection efficiency, low maintenance requirements, and considerable flexibility in terms of increasing the temperature of flue gases [6, 7]. Generally, ESPs may have a performance rate of removal particles over 99% while they consume a quite low energy [2, 8], however, they have limited effectiveness in removing microscopic particles [9].

* Supported by the Stipendium Hungaricum Scholarship.

Particles in an ESP are charged by gaseous ions generated by corona electrodes, and subsequently, they are are driven by electrical forces that gather these particles onto the collecting plates. Five processes comprise the electrostatic precipitation: ion generation by corona discharge; particle charging; particle mobility; accumulation of the dust particles to the collecting electrode; and removing accumulated dust particles [6, 10]. ESPs consist of parallel ducts with many corona wires within parallel grounding collecting electrodes. In ESPs, three physical factors engage: fluid flow, electrostatics, and particle mobility [2, 11]. Consequently, the conventional approach for removal of dust particles has relied heavily on fundamental concepts and laboratory studies [2, 11]. Because numerical technology for investigating complex physical processes has progressed, more effective and comprehensive numerical techniques for comprehending the electrical characteristics and particle movement in ESPs have been developed [2, 11]. When compared to practical approaches, numerical simulations are favored due to their versatility, affordability, and superior reliability [2, 12]. The efficiency of the collection process is significantly influenced by the configuration of the collecting electrodes and discharge wires. As a consequence of this, a number of researchers endeavoured to enhance the performance of ESPs by modifying the configuration of the collecting plates and discharge wires. According to boost the charging efficiency, researchers investigated electron charging, Ultraviolet photo charging, soft X-ray particle charging, and pulsed charging [2, 10]. Furthermore, it is stated that the shape of the collecting electrodes affects particle velocity and ESP's particle collection efficiency. Many experiments employed a large dust collector, the wider plate-spacing effect, to enhance dust removal performance; this effect depends on the configuration of the collecting plates in an ESP [2, 13].

Many investigations use the assumption that ground electrode geometries are as simple as a flat collecting plate. Meanwhile, some studies have been conducted to investigate the Electrohydrodynamic (EHD) flow in ESPs employing other configurations of collecting plates rather than the standard flat collecting plate [14–17]. Shen et al. investigated electrohydrodynamic flows in ESP with five electrode shapes [17]. Furthermore, numerical research was carried out to investigate the C-type collecting type, the corrugated shape, the triangular form, the W-type, and the crenelated type, where six different types of collecting electrodes were built using COMSOL software and compared to FPs [7]. The wavy pattern was also utilized to investigate electrical characteristics [6, 11, 18]. Corona discharge and particle motion have been the subject of several experimental and computational studies over the past few decades [8, 12, 19].

Corona discharge wires with different forms, diameters, and spacings have been tested in experimental and numerical ESP research [2, 6, 20, 21]. The number of discharge wires, which raises the corona current for the same voltage level, influences the performance of ESP in a variety of ways [2, 22, 23]. ESP current-voltage properties were also studied, and the influence of wire-to-wire distance was evaluated [2, 8, 24]. Also, Both Jedrusik et al. [25] and Gao et al. [12] studied the influence of corona wire shape on ESP collection efficiency. Additionally, Wang et al. [26] developed a spike-honeycomb form to examine the

effects of ionic wind on the flow field of air and particle precipitation. Based on FPs electrostatic precipitators (ESPs) with multiple wire electrodes, a numerical analysis was conducted on the charging and transport of microscopic particles, where modifications were done to the electrode configuration to improve the precipitator's particle capture by using three models of corona wires arrangements M1, M2 and M3 [27]. The majority of investigations were focused on ESPs with FPs collecting plates. However, the purpose of this research is to explore the W-type arrangement of collecting electrodes including three models of corona wires arrangements M1, M2, and M3 for a single-stage ESP. The results acquired with W-type are compared with FPs using the COMSOL Multiphysics simulation on the electric potential distribution, electric field distribution, current density distribution, space charge density distribution, and particle collection efficiency.

2 Mathematical Model

The mathematical model of the ESP involves corona discharge, gas movement, particle charging, and transportation. Consequently, the basic equations include the electric field and space charge, fluid flow, particle trajectory, charging, and collection efficiency equations, in that order.

2.1 Electric field and space charge

The numerical solution of the Poisson and charge-conservation equations gives the charge density and electric potential distribution of the ions within the ESP model. In this way, they might be summarized [28, 29]:

$$\frac{\partial \rho_q}{\partial t} + \nabla \bullet \mathbf{J} = 0 \tag{1}$$

$$\mathbf{J} = z_q \mu \rho_q \mathbf{E} + \rho_q \mathbf{u} \tag{2}$$

$$\varepsilon_0 \nabla^2 V = -\rho_q \tag{3}$$

$$\mathbf{E} = -\nabla \mathrm{V} \tag{4}$$

where ρ_q (C.m^{-3}) is the space charge number density, $\mathbf{J}$(A.m^{-2}) is the current density, z_q is the charge number, μ (m^2.V^{-1}.s^{-1}) is the ion mobility, $\mathbf{E}$(V.m^{-1}) is the electric field, $\mathbf{u}$(m.s^{-1}) is the fluid velocity, ε_0(F.m^{-1}) is the free-space permittivity, and V(V) is the electric potential [6, 28, 29].

These governing equations are used to calculate the electric potential and space charge density [2, 6]. These equations require the existence of boundary conditions, the first boundary is supplied by Peek's equation, which specifies the value of the electric field on the corona electrodes ($\mathbf{n} \bullet \mathbf{E} = E_0$), $\mathbf{n}$ is a normal unit vector [2, 6]. The second boundary conditions for Poisson's equation include ($V = 0$) at the collecting plates which are called grounding electrodes and a zero charge at the inlet and outlet [2, 6, 29, 30].

$$E_0 = 3 \times 10^6 \delta \cdot \left(1 + \frac{0.03}{\sqrt{\delta r_w}}\right) \tag{5}$$

$$\delta = \frac{T_0}{T}\frac{P}{P_0} \tag{6}$$

where E_0(V.m^{-1}) is the electric field on the corona electrode, r_w(m) is the corona wire radius, δ is a relation between T_0(293.15 K) the absolute temperature and P_0(760 mmHg) the normal atmospheric pressure and P and T are the operating values [2, 6].

2.2 Fluid flow

The ESP airflow is considered to have incompressible, steady-state, and homogeneous turbulence, which is characterized by the k-epsilon turbulence model [9, 29]. Meanwhile, in consideration of the effects of the electric field on the flow field, an electric field force element was added to the momentum equation. Following are the governing equations:

$$\rho \nabla \cdot \mathbf{u} = 0 \tag{7}$$

$$\rho \frac{\partial \mathbf{u}}{\partial t} + \rho\left(\mathbf{u}\cdot\nabla\right)\mathbf{u} = \nabla \cdot \left[-p\mathbf{I} + \mu\left(\nabla\mathbf{u} + \left(\nabla\mathbf{u}\right)^T\right)\right] + \mathbf{F}_{EHD} \tag{8}$$

$$\mathbf{F}_{EHD} = \rho_q \mathbf{E} \tag{9}$$

where ρ (kg.m^{-3}) is the fluid density, p (Pa) is the pressure, μ (kg.m^{-1}.s^{-1}) is the dynamic viscosity, and $\mathbf{F}_{EHD}$ is the electrohydrodynamic force [2, 6, 29].

2.3 Particle charging

The process of particle charging comprises the field charging and diffusion charging. It occurs when dust particles move through ionized gas in ESP, and in an electric field and ionized gas of high thermal motion of ions, respectively [7, 9, 29, 30]. It was employed the Lawless model in this study.

$$\tau_c \frac{dZ}{dt} = \begin{cases} \frac{V_s}{4\epsilon_0}\left(1 - \frac{V_e}{V_s}\right)^2 + f_a, & |V_e| \le |V_s|. \\ \frac{V_e - V_s}{e^{(V_e - V_s)} - 1} f_a, & |V_e| > |V_s|. \end{cases} \tag{10}$$

$$\tau_c = \frac{e^2}{4\pi\rho_q \mu k_B T_i} \tag{11}$$

where τ_c (s) is the charging time, Z is the accumulated charge number on each particle, k_B (J.K^{-1}) is the Boltzmann's constant, ε_0 (C.V^{-1}.m^{-1}) is the permittivity of a vacuum, e (C) is the electron charge, and T_i (K) is the ion temperature,

$$v_s = 3w_e \frac{\varepsilon_{r,p}}{\varepsilon_{r,p} + 2} \tag{12}$$

$$v_e = \frac{Ze^2}{4\pi\varepsilon_0 r_p k_B T_i} \tag{13}$$

$$w_e = \frac{e r_p |E|}{k_B T_i} \tag{14}$$

where v_e is the self-potential of the particle, w_e is the dimensionless electric field intensity, r_p (m) is is the particle radius, $\varepsilon_{r,p}$ is the relative permittivity of the particles, f_a is an analytic fitting function which is depending on w_e [29, 31].

$$f_a(w_e) = \begin{cases} \frac{1}{(w_e+0.475)^{0.575}}, & w_e \geqslant 0.525. \\ 1, & w_e < 0.525. \end{cases} \tag{15}$$

2.4 Particle Kinetics

A charged particle is subjected to both a drag force from fluid flow and an electrical force from the electric field. Despite this, the gravitational force is still there, but because to the tiny particle sizes, it may be ignored. It is therefore possible to determine the particle's velocity using Newton's second law by considering its drag and electric forces [7, 14, 29]. The drag force is proportional to the mass of the particle and the speed difference between the particle and the fluid; a correction factor is also applied to account for additional effects owing to particle size. The Cunningham-Millikan-Davis model is used to explain this adjustment [7, 14, 29]

$$\frac{d\mathbf{x}}{dt} = \mathbf{v} \tag{16}$$

$$\frac{d}{dt}(m_p\mathbf{v}) = \mathbf{F}_D + \mathbf{F}_e \tag{17}$$

where $\mathbf{x}$(m) is the particle position,$\mathbf{v}$ (m.s^{-1}) is the particle velocity, m_p (kg) is the particle mass, $\mathbf{F}_D$ (N) is the drag force, and $\mathbf{F}_e$ (N) is the electric force,

$$\mathbf{F}_D = \frac{1}{\tau_p S} m_p(\mathbf{u} - \mathbf{v}) \tag{18}$$

$$\tau_p = \frac{4\rho_p d_p^2}{3\mu C_D Re_r} \tag{19}$$

$$\mathbf{F}_e = eZ\mathbf{E} \tag{20}$$

where τ_p (s) is the particle velocity-time response; S is the drag correction coefficient, ρ_p (kg.m^{-3}) is the density of the particles; d_p (m) is the particle diameter; C_D is the Cunningham correction factor; and R_{e_r} is the Reynolds number , e (C) is an elementary charge, and Z is the accumulated charge number on the particle [6, 7, 14, 29].

2.5 Particle collection efficiency

Deutsch, an early scientific researcher, proposed that the structure of an exponential function as a mathematical formula affected the performance or efficiency of an ESP equation (21):

$$\eta = 1 - \exp\left(-\frac{L.|\mathbf{v}|}{s.|\mathbf{u}|}\right) \tag{21}$$

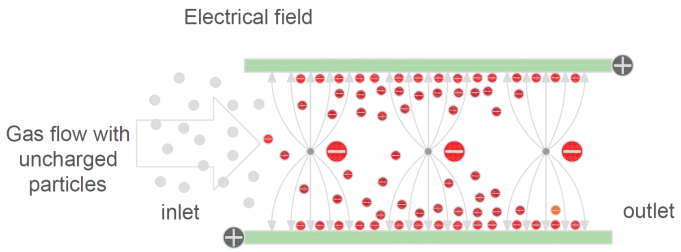

Fig. 1. The principle work of ESPs.

where, L(m), the separation between a corona and one of the collecting plates s(m), and the fluid and dust particle's movement velocities [2, 6, 18, 29, 32]. Numerically, the collection efficiency is calculated for the purpose of this study by utilizing a particle counter that is placed on the outlet of the ESP model.

3 Numerical Model

3.1 The principle work of ESPs

The electrostatic precipitator creates typical multi-physical field phenomena through the interplay of gas flow, electric field, and dust particle motion [2, 7]. The action of ESP is depicted in simplified form in Fig. 1. There are two electrode sets in an ESP: negative discharge wires connected to a negative DC supply and positive collection electrodes coupled to a positive DC source [2, 7]. As soon as the ESP activates, the corona influences the air molecules, which results in an abundance of free electrons and ions in the airflow [2, 7]. When dusty air passes through the ESP, the free electrons available between the electrodes collide with the dust particles [2, 7]. Because of the free electrons attached to them, the dust particles will have a negative charge. Charged dust particles are drawn to positive-charged collecting plates by electric fields. The dust particles gathered on the collecting plates are cleared by rapping them [2, 7].

3.2 ESP modeling settings

By using COMSOL Multiphysics simulation, a variety range of boundary value problems was handled using the finite element method (FEM) [2]. The properties listed in Table 1 were employed and related to a previous paper [2]. The objective of this investigation is to explore the W-type arrangement of collecting electrodes including three models of corona wires arrangements M1, M2, and M3 with a single stage of an ESP. The ESP's gas flow was dependably considered as a fixed typical k-ϵ turbulent flow in this paper. The collecting plates are located on the top and bottom plates, respectively, and the positions of corona wires are on

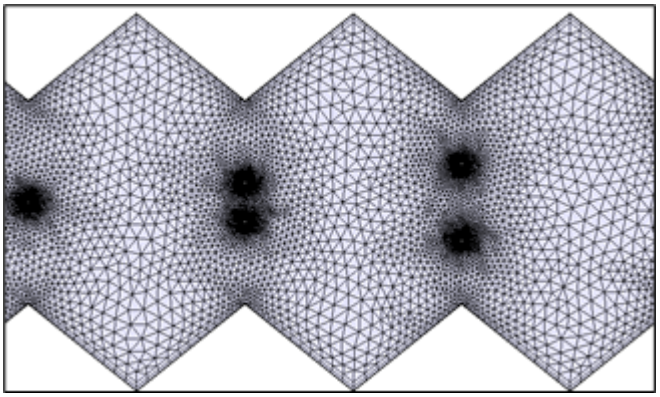

Fig. 2. Mesh grid of case M3 for w-type.

the x-axis for case M1, the x-axis for 3 corona wires, and $y = \pm 23$ mm for the last 2 corona wires for case M2, and the x-axis for the first corona wire and 2 corona wires at $y = \pm 23$ and 2 corona wires at $y = \pm 43$ mm for case M3. Fig. 2 illustrates the mesh case M3 w-type using COMSOL. The fluid's inlet is stated on the left side. In contrast, the ESP's outlet is on the right side. The particles were pushed into the fluid flow at the ESP inlet, with a mass density of 2200 (kg/m^3) and a particle relative permittivity of 5 and the particles ranged in radius from 0.01 to 5 μm [2, 6].

Fig. 3 represents the geometrical configuration for FPs and w-type collecting electrodes for M1, M2 and M3, All of the results produced and presented in this study are based on the $y = 50$ mm cutting line depicted in blue colour. Fig. 4 depicts the electrical potential distributions for three cases M1, M2, and M3 for FPs and W-type, where maximum values on discharge electrode surfaces decrease towards collecting electrodes in an asymmetrical amplitude distribution.

4 RESULTS AND DISCUSSION

The results obtained were divided into three study groups for FPs and w-type: case M1, case M2, and case M3; case M1 refers to the use of 5 corona wires on the x-axis, while case M2 refers to the use of 5 corona wires, 3 corona wires are located in the same position of M1, but the last two corona wires are located parallel at $y = \pm 23$ mm. In case of M3, the first corona wire is located at the same place for M1 and M2, but the 2^{nd} and the 3^{rd} corona wires are located at $y = \pm 23$ mm, and the 4^{th} and the 5^{th} are positioned at $y = \pm 43$ mm. Nevertheless, previous research has described the connection between the results obtained using FPs and w-type for a variety of positions of corona wires [2, 33]. The numerical electrical potential distribution results and the experimental data acquired by Penney were compared to confirm if the suggested model is

Table 1. Specifications Parameters for the 3 cases of W-type.

Description	Values
Length, (mm)	750
The space between the collecting electrodes, (mm)	150
The gap space between 2 corona wires, (mm) M1	x=112.5
The gap space between 2 corona wires, (mm) M2	x=112.5 and y=23
The gap space between 2 corona wires, (mm) M3	x=112.5 , y_1=23, y_2=43
The number of corona wires	5
Corona wire radius, (mm)	0.75
The voltage applied, (kV)	45
The fluid velocity, (m/s)	1
Temperature, (K)	293.15
Pressure, (atm)	1
Gas density, (kg·m^{-3})	1.2
Gas viscosity, (Pa·s)	1.85×10^{-5}

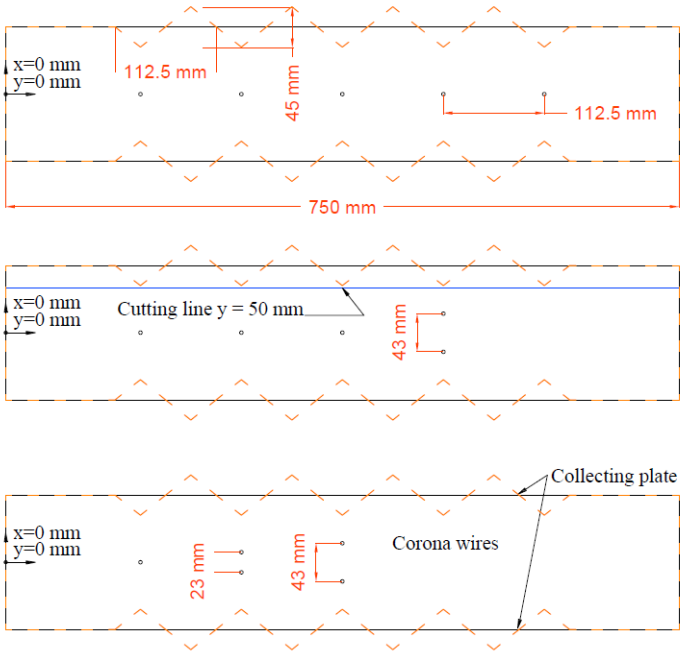

Fig. 3. Geometrical arrangement for w-type colleting plates.

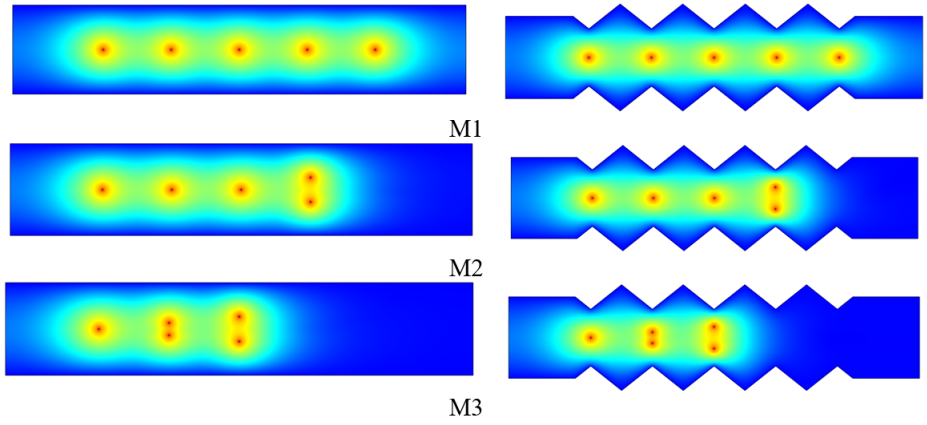

Fig. 4. Electrical potential and space charge density distributions for M1, M2, and M3 respectively.

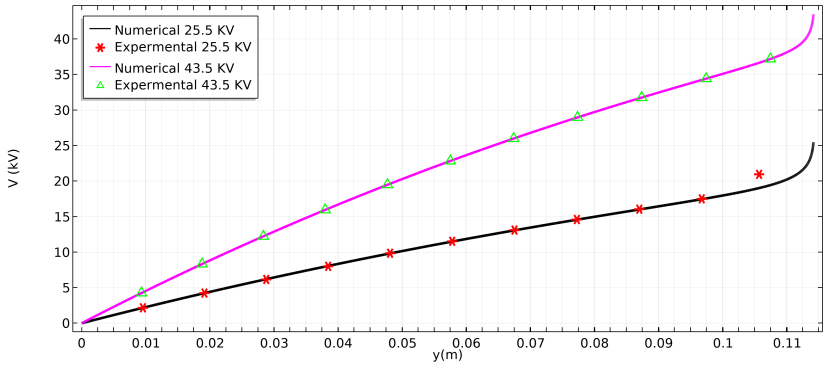

Fig. 5. The electrical potential validation between numerical and experimental data.

accurate. The geometric and model parameters were determined in the Penney's research, where the corona wire radius was 0.1524 mm , 152.4 mm was the distance between two corona wires, and 228.6 mm was the width and 609 mm was the length and by using 4 corona wires [34]. A close representation of the data is reflected in the results. Fig. 5 shows the validation of this study in the electrical potential with the range 25.5-43.5 KV.

4.1 The Electric Field Distribution

In general, the magnitude of the electric field along the distribution of the corona wires is the highest, while the lowest is between the corona wires with respect

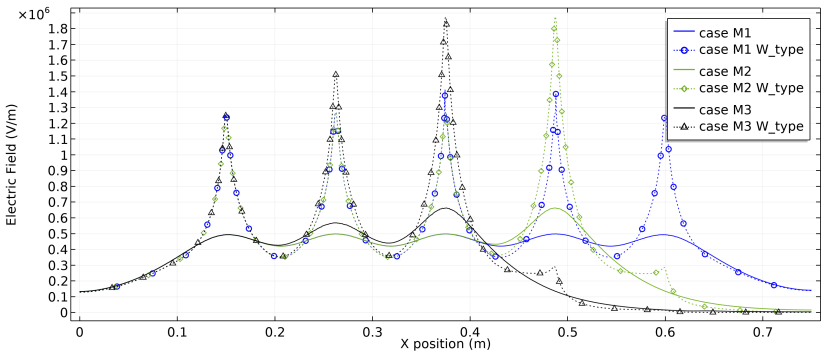

Fig. 6. The distribution of electrical field for M1,M2 and M3.

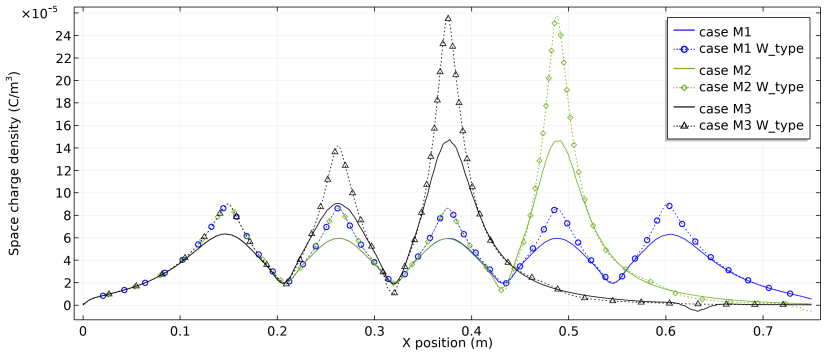

Fig. 7. Space charge distribution for M1,M2 and M3.

to x-axis. As shown in Fig.6 with using the cutline $y = 50$ mm, the electrical field magnitudes for w-type in all cases are greater than for FPs based on the same position. The curves for case M1 FPs and w-type are more uniform than case M2 and M3 based on the position of parallel corona wires 4^{th} and 5^{th} for case M2, and 2^{nd} ,3^{rd}, 4^{th}, and 5^{th} for case M3. At $x = 0.375$ m, the highest electrical field magnitude is 1.8×10^6 V for case M3 w-type because it was used 2 corona wires in this position with 43 mm distance.

4.2 The Space Charge Density Distribution

The space charge density distribution for case M1, M2 and M3 is demonstrated in Fig.7, for all cases, the highest values of magnitude are presented when using multiple corona wires for case M3 w-type at $x = 0.375$ m and M2 w-type at $x = 0.4875$ m with $24 \times 10^{-5}(\text{C/m}^3)$.

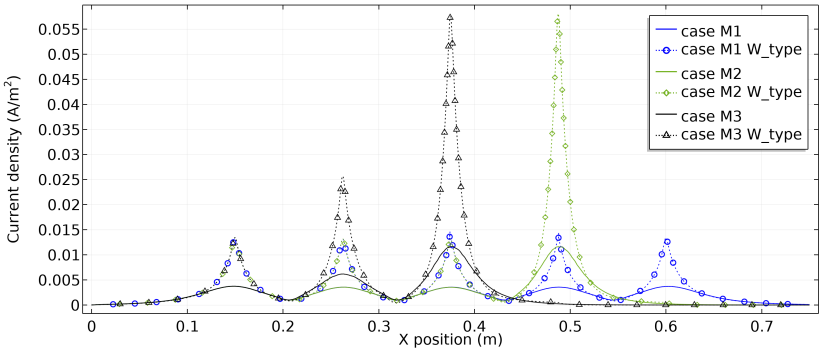

Fig. 8. Current density distribution for M1, M2 and M3.

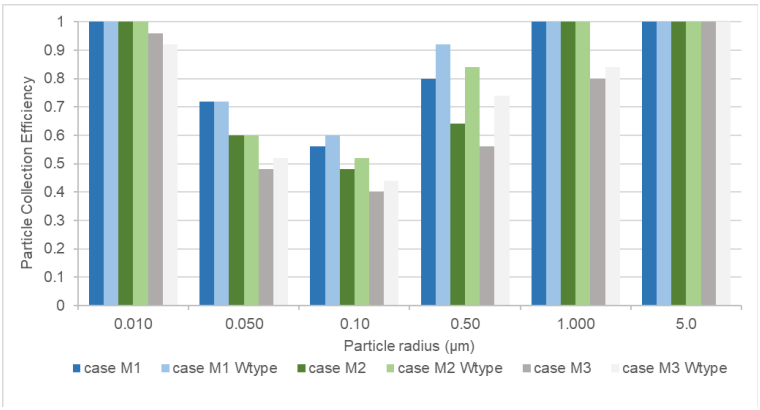

Fig. 9. Particle collection efficiency using w-types collecting plates.

4.3 The Current Density Distribution

Greater values of current density are demonstrated for all cases M2, and M3 for w-type and if they are compared with FPs, see Fig.8, about 0.055 A/m^2 at $x = 0.4875$ and $x = 0.375$ m, respectively. While case M1 is the most uniform current density distribution due to the arrangement of corona electrodes on the x-axis, then it is followed by case M1 w-type.

4.4 ESP's Particle Collection Efficiency

The results of ESP's particle collection efficiency by using cases M1, M2 and M3 for the particles range 0.01 to 5 μm are indicated in Fig.9. They are compared to FPs M1, M2 and M3 cases to estimate the effect of using multiple corona electrodes on the particle collection efficiency. Case M1 has the highest efficiency

magnitudes based on the results. Higher ESP's efficiency magnitudes in this study are attained with the case M1 for particles range 0.05 to 0.5 μm. In the range (0.1 to 0.5 μm), the ESP's particle collection efficiency values of using M1, M2, and M3 for w-type are higher than using FPs.

5 CONCLUSIONS

Using w-types collecting plates for 3 cases: M1, M2, and M3, this paper aimed to explore the W-type designs of collecting plates including three models of corona wires arrangements M1, M2, and M3 in a single-stage ESP. The results gained with W-type are corresponded with FPs using the COMSOL Multiphysics simulation on ESP electrical properties. The following are the main conclusions:

- Case M1 describes the use of 5 corona wires on the x-axis, while case M2 describes the use of 5 corona wires, 3 corona wires are in the same position as M1, but the last two corona wires are located parallelly at $y = \pm 23$ mm. In the case of M3, the first corona wire is located at the same place for M1 and M2, but the 2^{nd} and the 3^{rd} corona wires are located at $y = \pm 23$ mm, and the 4^{th} and the 5^{th} are positioned at $y = \pm 43$ mm.
- Maximum values of the electrical potential on corona wire surfaces decrease towards collecting plates in an asymmetrical amplitude distribution.
- With using the cutline $y = 50$ mm, the electrical field magnitudes for w-type in all cases are greater than for FPs. The curves for case M1 FPs and w-type are more uniform than case M2 and M3 based on the position of parallel corona wires 4^{th} and 5^{th} for case M2, 2^{nd} , 3^{rd} , 4^{th} , and 5^{th} for case M3.
- For all cases, the highest values of space charge and current density are presented when using multiple corona wires for case M3 w-type at $x = 0.375$ m and M2 w-type at $x = 0.4875$ m.
- Case M1 has the highest efficiency magnitudes based on the results. Higher ESP's efficiency magnitudes in this study are attained with the case M1 for particles range 0.05 to 0.5 μm.

Finally, this study is linked to other ESP research in our current research plan; while new ESP studies are being conducted, the goal of this study is to enhance and work collaboratively with future ESP research, with future work evaluating various geometries configurations to improve the collection efficiency.

References

1. Perera, F.P.: Multiple threats to child health from fossil fuel combustion: impacts of air pollution and climate change. Environmental health perspectives 125, 141–148 (2017)
2. Fayyad, M.B., González, A.A., Iváncsy, T.: Numerical study of a duct-type esp with w-type collecting electrodes and different circular corona electrodes radius. In: 2022 8th International Youth Conference on Energy (IYCE). pp. 1–5 (2022)

3. Mizuno, A.: Electrostatic precipitation. IEEE Transactions on Dielectrics and Electrical Insulation 7, 615–624 (2000)
4. Zheng, C., Wang, Y., Liu, Y., Yang, Z., Qu, R., Ye, D., Liang, C., Liu, S., Gao, X.: Formation, transformation, measurement, and control of so3 in coal-fired power plants. Fuel 241, 327–346 (2019)
5. Liang, Y., Li, Q., Ding, X., Wu, D., Wang, F., Otsuki, T., Cheng, Y., Shen, T., Li, S., Chen, J.: Forward ultra-low emission for power plants via wet electrostatic precipitators and newly developed demisters: Filterable and condensable particulate matters. Atmospheric Environment 225, 117372 (2020)
6. Asipuela, A., Fayyad, M.B., Iváncsy, T.: Study and numerical simulation of a duct-type esp with wavy collecting electrodes and different circular corona electrodes radius. In: 2022 IEEE 4th International Conference on Dielectrics (ICD). pp. 234–238 (2022)
7. Zhou, W., Jiang, R., Sun, Y., Chen, B., Liu, B.: Study on multi-physical field characteristics of electrostatic precipitator with different collecting electrodes. Powder Technology 381, 412–420 (2021)
8. Wang, Y., Zhang, H., Gao, W., Shao, L., Wu, Z., Zhao, Z., Ge, C., Hu, D., Zheng, C., Gao, X.: Improving the removal of particles via electrostatic precipitator by optimizing the corona wire arrangement. Powder Technology 388, 201–211 (2021), https://www.sciencedirect.com/science/article/pii/S0032591021003740
9. Wang, X.: Effects of corona wire distribution on characteristics of electrostatic precipitator. Powder Technology 366, 36–42 (2020), https://www.sciencedirect.com/science/article/pii/S0032591020301480
10. Lee, G.H., Hwang, S.Y., Cheon, T.W., Kim, H.J., Han, B., Yook, S.J.: Optimization of pipe-and-spike discharge electrode shape for improving electrostatic precipitator collection efficiency. Powder Technology 379, 241–250 (2021), https://www.sciencedirect.com/science/article/pii/S0032591020309931
11. Choi, H.Y., Park, Y.G., Ha, M.Y.: Numerical simulation of the wavy collecting plate effects on the performance of an electrostatic precipitator. Powder Technology 382, 232–243 (2021)
12. Gao, W., Wang, Y., Zhang, H., Guo, B., Zheng, C., Guo, J., Gao, X., Yu, A.: Numerical simulation of particle migration in electrostatic precipitator with different electrode configurations. Powder Technology 361, 238–247 (2020)
13. Ko, J.H., Ihm, S.K.: A two-dimensional model for polydisperse particles on the effective migration rate of the electrostatic precipitator with wider plate-spacing. Aerosol science and technology 26, 398–402 (1997)
14. Asipuela, A., Iváncsy, T.: Study and numerical simulation of the electrical properties of a duct-type electrostatic precipitator using seven circular corona wires: A review. Periodica Polytechnica Electrical Engineering and Computer Science 66, 286–293 (2022), https://pp.bme.hu/eecs/article/view/19482
15. Wen, T.Y., Krichtafovitch, I., Mamishev, A.V.: Numerical study of electrostatic precipitators with novel particle-trapping mechanism. Journal of Aerosol science 95, 95–103 (2016)
16. Zhu, Y., Gao, M., Chen, M., Shi, J., Shangguan, W.: Numerical simulation of capture process of fine particles in electrostatic precipitators under consideration of electrohydrodynamics flow. Powder Technology 354, 653–675 (2019)
17. Shen, H., Yu, W., Jia, H., Kang, Y.: Electrohydrodynamic flows in electrostatic precipitator of five shaped collecting electrodes. Journal of Electrostatics 95, 61–70 (2018)

18. Asipuela, A., Fayyad, M.B., Iváncsy, T.: The effect of corona wire position and radius in a duct-type esp with wavy collecting plates. International Journal of Electrical and Electronic Engineering Telecommunications 11, 262–268 (7 2022)
19. Tong, Y., Liu, L., Zhang, L., Bu, S., Chen, F., Shao, W., Feng, C., Xu, W., Qi, S., Fu, L.: Separation of fine particulates using a honeycomb tube electrostatic precipitator equipped with arista electrodes. Separation and Purification Technology 236, 116299 (2020), https://www.sciencedirect.com/science/article/pii/S1383586619330126
20. Yan, P., Zheng, C., Xiao, G., Xu, X., Gao, X., Luo, Z., Cen, K.: Characteristics of negative dc corona discharge in a wire–plate configuration at high temperatures. Separation and Purification Technology 139, 5–13 (2015), https://www.sciencedirect.com/science/article/pii/S1383586614006388
21. Xu, X., Zheng, C., Yan, P., Zhu, W., Wang, Y., Gao, X., Luo, Z., Ni, M., Cen, K.: Effect of electrode configuration on particle collection in a high-temperature electrostatic precipitator. Separation and Purification Technology 166, 157–163 (2016), https://www.sciencedirect.com/science/article/pii/S138358661630226X
22. Said, H.A., Aissou, M., Nouri, H., Zebboudj, P.Y.: Effect of wires number on corona discharge of an electrostatic precipitators. Journal of Electrical Systems 10, 392–405 (2014)
23. Said, H.A., Nouri, H., Zebboudj, Y.: Analysis of current-voltage characteristics in the wires-to-planes geometry during corona discharge. The European Physical Journal-Applied Physics 67 (2014)
24. Khaled, U., Eldein, A.Z.: Experimental study of v–i characteristics of wire–plate electrostatic precipitators under clean air conditions. Journal of Electrostatics 71, 228–234 (2013)
25. Jedrusik, M., Swierczok, A., Teisseyre, R.: Experimental study of fly ash precipitation in a model electrostatic precipitator with discharge electrodes of different design. Powder Technology 135, 295–301 (2003)
26. Wang, Y., Gao, W., Zhang, H., Huang, C., Luo, K., Zheng, C., Gao, X.: Insights into the role of ionic wind in honeycomb electrostatic precipitators. Journal of Aerosol Science 133, 83–95 (2019)
27. Dong, M., Zhou, F., Zhang, Y., Shang, Y., Li, S.: Numerical study on fine-particle charging and transport behaviour in electrostatic precipitators. Powder Technology 330, 210–218 (2018)
28. Potrymai, E., Perstnov, I.: Time dependent modelling and simulation of the corona discharge in electrostatic precipitators (2014)
29. Multiphysics, C.: Electrostatic precipitator (2018), https://www.comsol.com/model/electrostatic-precipitator-71361
30. Rubinetti, D., Weiss, D., Egli, W.: Corona discharge–a fully coupled numerical approach verified and validated. The International Journal of Multiphysics 11, 375–386 (2017)
31. Zheng, C., Zhang, X., Yang, Z., Liang, C., Guo, Y., Wang, Y., Gao, X.: Numerical simulation of corona discharge and particle transport behavior with the particle space charge effect. Journal of Aerosol Science 118, 22–33 (2018)
32. Świerczok, A., Jędrusik, M.: The collection efficiency of esp model - comparison of experimental results and calculations using deutsch model. Journal of Electrostatics 91, 41–47 (2018), https://www.sciencedirect.com/science/article/pii/S0304388617303029
33. Fayyad, M.B., González, A.A., Iváncsy, T.: The effects of the corona wire distribution with w-type of collecting plates on the characteristics of electrostatic precipi-

tators. presented at 2022 International Conference on Energy Storage Technology and Power Systems ESPS 2022) (2 2022)
34. He, Z., Dass, E.T.: Correlation of design parameters with performance for electrostatic precipitator. part i. 3d model development and validation. Applied Mathematical Modelling 57, 633–655 (5 2018)